Interaction of $Y_Z^{\bullet}$ with Its Environment in Acetate-Treated Photosystem II Membranes and Reaction Center Cores

Pierre Dorlet,† Marilena Di Valentin, Gerald T. Babcock, and John L. McCracken*

Department of Chemistry, College of Natural Sciences, Michigan State University, East Lansing, Michigan 48824

Received: March 24, 1998; In Final Form: June 16, 1998

The photosynthetic oxidation of water to oxygen occurs in photosystem II (PSII) at an active site composed of a tetranuclear cluster of manganese ions, a redox active tyrosine, Y_Z, and two essential cofactors, calcium and chloride. Recently, several experimental observations have led to the proposal of a metalloradical catalytic cycle in which water oxidation occurs via hydrogen-atom abstraction by the tyrosyl radical from water bound to the manganese cluster. This model predicts a close proximity between the radical tyrosine, $Y_z^{\bullet}$, and the Mn cluster and the involvement of the radical in a bifurcated hydrogen bond. Magnetic resonance techniques have been used in this work to probe the interaction of the tyrosyl radical with its environment in PSII samples in which the catalytic cycle is blocked by acetate treatment and the enzyme is trapped in a paramagnetic $S_2Y_z^{\bullet}$ state. Radical interaction with the metal cluster has been studied via simulations of the EPR spectra obtained for this state. The simulations were based on a radical-pair model and included terms for both electron−electron dipolar and exchange interactions. The results show a dominant exchange interaction between the radical and the manganese cluster in these preparations and led to an estimate of 8−9 Å for the spin−spin distance. ESEEM spectroscopy and $^1H_2O/^2H_2O$ exchange were used to study interactions of the $S_2Y_z^{\bullet}$ state with exchangeable hydrogen nuclei in the site. Two-pulse ESEEM data show features expected for a radical-pair species, in support of our analysis of the continuous-wave EPR spectrum. An ESEEM analysis based on an electron spin $^1/_2$, nuclear spin 1 model shows that both two- and three-pulse ESEEM data are consistent with four deuterons that exhibit an electron−nuclear dipole−dipole coupling of 0.42 MHz. The validity of this analysis and its implications for the oxygen-evolving apparatus are discussed.

Introduction

Photosystem II (PSII) in green plants and cyanobacteria uses light to split water and evolve molecular oxygen.[1] Photon absorption in PSII and subsequent charge separation produce oxidizing equivalents that are transferred to the oxygen-evolving complex (OEC), which comprises a cluster of four manganese ions and a redox-active tyrosine, Y_Z, in close physical proximity.[2] Recent work has led to the proposal that the transfer of oxidizing equivalents occurs by $Y_Z^{\bullet}$-mediated hydrogen-atom abstraction from substrate water bound to the $(Mn)_4$ ensemble.[2,3] The oxidizing equivalents transferred in this atom abstraction process are ultimately stored as increasingly oxidized manganese species. During the catalytic cycle, the OEC goes through four oxidation steps before water can be split and molecular oxygen released. The different intermediates that occur in this process are called the S_n states where n varies from 0 to 4 and denotes the overall oxidation state of the OEC. The dark stable state is S_1. In the S_2 state, the paramagnetic manganese cluster exhibits an EPR spectrum called the multiline signal (hereafter called normal multiline) that spans roughly 1900 G and is composed of about 20 lines arising from hyperfine interactions with the manganese cluster.[4] This signal can be accumulated by illuminating oxygen-evolving samples at 200K.

In addition to Y_z and the $(Mn)_4$ cluster, water oxidation requires two other cofactors, Ca^{2+} and Cl^-. In preparations inhibited by the depletion of either of these cofactors, the $S_2 \rightarrow S_3$ transition is blocked[5] and the system is locked in a paramagnetic $S_2Y_z^{\bullet}$ configuration in which the tyrosyl EPR signal is broadened by its magnetic interaction with the manganese cluster. This $S_2Y_z^{\bullet}$ signal, also called the "split signal", was first discovered in Ca^{2+}-depleted preparations,[6] and its assignment to $Y_z^{\bullet}$ interacting magnetically with the $(Mn)_4$ cluster was made recently.[7] The nature of the magnetic interaction between the two species is under debate, however, and mechanisms that invoke either primarily dipolar[2a,8] or primarily exchange[9,10] interaction have been reported. In the work by MacLachlan and co-workers, extensive simulations of $S_2Y_z^{\bullet}$ signals from various inhibited preparations were made and the exchange interaction was found to be the dominant contribution. Addition of acetate to PSII preparations is one of the treatments that inhibits the system on the $S_2 \rightarrow S_3$ transition, supposedly by depleting the Cl^- cofactor.[11] This treatment is similar to Ca^{2+} depletion, as an $S_2Y_z^{\bullet}$ species is produced. The EPR spectrum of this inhibited state, however, differs from that of the Ca^{2+}-depleted preparations, as two satellite peaks along with an underlying multiline signal accompany the main $S_2Y_z^{\bullet}$ signal. These extra features provide more constraints for computer simulations. We have investigated the nature of the magnetic interactions by simulating the continuous-wave EPR spectrum of the $S_2Y_z^{\bullet}$ signal obtained in acetate-treated preparations.

* Corresponding author. Fax: 517-353-1793. E-mail: mccracke@pilot.msu.edu.

† Present address: DBCM/SBE Bat 532, CEN Saclay, 91191 Gif-sur-Yvette cedex, France.

S1089-5647(98)01609-5 CCC: $15.00 © 1998 American Chemical Society
Published on Web 08/13/1998

The OEC was further studied in acetate-treated PSII membranes and reaction center cores to assess bulk water accessibility to the paramagnets in the $S_2Y_z^\bullet$ state. This was done to provide insight into the structure of the site and into H-bonding to $Y_z^\bullet$ in the presence of the $(Mn)_4$ cluster. Electron spin−echo envelope modulation (ESEEM) on ^2H_2O-exchanged samples was used to quantitate exchangeable protons and ambient water in close proximity of the $(Mn)_4-Y_z^\bullet$ entity. Similar studies have been done by Britt and co-workers also in acetate-treated samples[8] and by Tommos et al. in calcium-depleted and manganese-depleted preparations.[12] They both found that in the presence of the $(Mn)_4$ cluster, two protons were hydrogen-bonded to the tyrosyl radical. Here, a detailed analysis of both two- and three-pulse ^2H-ESEEM data was undertaken to define the number of exchangeable nuclei and their distance from the paramagnetic center in the acetate-treated system more clearly. The analysis of the EPR spectrum, combined with constraints provided by the relative "damping" or line widths of the ^2H-matrix and sum-combination peaks as observed in two-pulse ESEEM spectra of $S_2Y_z^\bullet$, suggest that refinements to the $S = {}^1/_2$, $I = 1$ models to analyze the $S_2Y_z^\bullet$ ESEEM data may be required.

Experimental Section

Sample Preparation. All biochemical preparations were performed in a cold room (4 °C) under dim green light. Photosystem II membranes (BBYs) were prepared as described.[13] The preparations were frozen at a chlorophyll concentration of about 8 mg_{Chl}/mL and stored at −80 °C until used. Photosystem II reaction center cores (RCC) were prepared by following the method developed by Mishra and Ghanotakis[14] with modifications (D. Ghanotakis, personal communication). For this improved procedure, BBYs were diluted to a chlorophyll concentration of 1 mg_{Chl}/mL in SMN (sucrose 0.4 M, MES 50 mM, pH 6.0, sodium chloride 15 mM) buffer, and an equal volume of 0.8% OTG detergent in SMN was added. The resulting mixture was incubated 10 min on ice in complete darkness. It was then diluted in a 2:1 ratio with SMN buffer containing 30 mM $MgCl_2$ and further incubated for 5 min in the dark. The preparation was centrifuged for 30 min at 20 000 rpm in a Sorvall SS34 rotor. The supernatant was diluted in a 2:1 ratio with MN (MES 50 mM, pH 6.0, sodium chloride 15 mM) buffer and centrifuged for 40 min at 20 000 rpm. The pellet was resuspended in SMN buffer. An additional washing with SMN buffer pH 5.5 was done for samples meant to be acetate treated. The polypeptide content of the preparations was assayed with SDS-page electrophoresis gel (data not shown). Oxygen evolution was measured by using a Clark type O_2 electrode; the assay buffer was SMN for BBY preparation and SMN, with 10 mM $CaCl_2$ added, for RCC preparation. DCBQ (200 μM) and ferricyanide (500 μM) were added as exogenous electron acceptors. The O_2 evolution rates were typically 750−800 $\mu mol_{O_2}/mg_{Chl}/h$ for BBY membranes and 1500 $\mu mol_{O_2}/mg_{Chl}/h$ for RCC.

Acetate treatment was carried out by washing the BBY preparation twice with SMN buffer pH 5.5 containing 0.5 M acetate. In the case of RCC, the acetate was simply injected from a 5 M stock solution, equilibrated at pH 5.5, to a final concentration of 0.5 M. No prewashing in acetate buffer was required in order to induce the maximum $S_2Y_z^\bullet$ signal in these more resolved preparations. After treatment, the O_2 evolution rate measured at pH 5.5 in the presence of 0.5 M acetate was 0. After repletion (sample put in acetate-free SMN buffer at pH 6.0 in the presence of 20 mM $CaCl_2$), the O_2 evolution rate was 95% of the control.

^2H_2O exchange was carried out as follows: For BBY, SM buffer, pD 5.5 in ^2H_2O, was used to wash the pellet that resulted from the Triton step 3 times; 0.5 M deuterated acetate was present in the buffer for the last two washings. The last resuspension was done to a final concentration of 6 mg_{Chl}/mL. For RCC, the pellet of cores was washed twice with SM buffer, pD 5.5 in ^2H_2O. The last resuspension was done to a final concentration of about 4 mg_{Chl}/mL. In all cases, the PS II preparation was in the presence of ^2H_2O for at least 45 min prior to illumination.

Samples were put in calibrated quartz EPR tubes along with 0.5 mM PPBQ as an electron acceptor. Illumination in order to generate the $S_2Y_z^\bullet$ state was performed by using 400 W IR filtered lamps for 10 s at 273 K followed by 15 s of additional illumination as the temperature was lowered to about 180 K in an ethanol bath cooled with liquid nitrogen. Dark adaptation to allow the decay of the $S_2Y_z^\bullet$ state so that the background contribution could be recorded was done by leaving the sample at 193 K in complete darkness for 48 h. The absence of the $S_2Y_z^\bullet$ signal in dark-adapted samples was checked with CW-EPR.

EPR Spectroscopy. CW-EPR spectra were recorded with a TE_{102} mode cavity at liquid helium temperatures on a Bruker ESP-300e X-band spectrometer equipped with an ESR 900 cryostat and a GSP 600 transfer line from Oxford Instruments. The microwave frequency was measured with an EIP model 25B frequency counter connected to the microwave bridge.

ESEEM Spectroscopy. ESEEM spectra were recorded by using a home-built spectrometer.[15] The microwave cavity used for these measurements utilized a folded-stripline resonator[16] and a Gordon coupling arrangement similar to that developed by Britt and Klein.[17] The sample temperature was 1.8 K for all measurements. Two-pulse ESEEM experiments were performed by measuring the integrated intensity of the electron spin−echo as a function of the time τ separating the two pulses in the Hahn sequence: $\pi/2 - \tau - \pi$. Three-pulse ESEEM experiments were accomplished by using the stimulated echo sequence, $\pi/2 - \tau - \pi/2 - T - \pi/2$, where the time T is varied.[18] All spectra were recorded on illuminated and subsequently annealed samples, and the difference was taken to remove the contribution from the background and obtain the envelope modulation arising from the $S_2Y_z^\bullet$ state. Care was taken in optimizing the sample tube position and microwave resonator coupling to ensure that constant spectrometer gain/sensitivity was maintained for these measurements.

Three-pulse ESEEM experiments were run at a τ value that maximized the modulations arising from deuterium nuclei.[19] Dead-time reconstruction of the time domain data was performed by following the Mims' procedure,[20] except that peak correction factors (see ref 20, eq 13) were calculated directly from the transformed spectra and entered into an interactive windowing procedure. The frequency-domain spectra were obtained by cosine Fourier transformation of the time-domain data. Simulations of ESEEM spectra were based on the formalism developed by Mims[21] and carried out on a personal computer with the Matlab 5.0 program from The Mathworks Inc. (Natick, MA).

Results

CW-EPR. Figure 1 shows the EPR signal arising from the $S_2Y_z^\bullet$ state obtained in acetate-treated PS II RCCs after illumination at 273 K. The two major features of the $S_2Y_z^\bullet$ EPR signal are split by 21 mT and centered at about $g = 2.00$. The central part of this spectrum is masked by the presence of

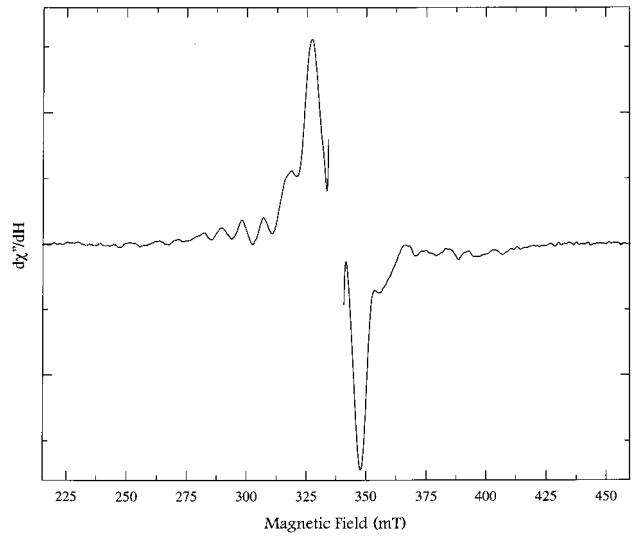

Figure 1. Light minus-annealed continuous-wave EPR spectrum of the $S_2Y_z^{\bullet}$ paramagnetic center in an acetate-treated PSII reaction center core. The central part overlapping with the signal of Y_D has been removed. Experimental conditions: $\nu_{mw} = 9.464$ GHz; power = 20 mW; modulation amplitude = 20 G; time constant = 80 ms; scan time = 320 s; $T = 7$ K; average of five scans.

the intense signal from $Y_D^{\bullet}$. The major features of the $S_2Y_z^{\bullet}$ EPR signal are accompanied by two satellite peaks, also centered at $g = 2.00$ and separated by approximately 38 mT, along with an underlying multiline signal from the S_2 state of the manganese cluster. This multiline signal is different from the one arising from the S_2 state of untreated O_2-evolving samples and has been observed along with the split signal only in acetate-treated samples[22,23] so far. In acetate-treated PSII membranes, the signal arising from the $S_2Y_z^{\bullet}$ state is essentially the same but the splitting is somewhat broader, 23 mT for the major features and 44 mT for the satellite peaks (see Figure 2 and refs 22 and 23). The underlying multiline signal is also present in this case, although it does not appear clearly in the experimental spectrum of Figure 2 because of the experimental conditions. We have mainly used RCCs to study the signal because of the higher spin concentration obtained in these more resolved PS II preparations.

Previous work on the analysis of the $S_2Y_z^{\bullet}$ signal modeled the electron−electron interaction between S_2 and $Y_z^{\bullet}$ with primarily dipolar coupling[2a,8] or primarily isotropic exchange coupling.[9,10] The Hamiltonian we used was the following:

$$\hat{H} = g_{Y_z}\beta\hat{\mathbf{S}}_{Y_z}\cdot\mathbf{H} + g_{(Mn)_4}\beta\hat{\mathbf{S}}_{(Mn)_4}\cdot\mathbf{H} + (\hat{\mathbf{I}}_1A_1 + \hat{\mathbf{I}}_2A_2 + \hat{\mathbf{I}}_3A_3 + \hat{\mathbf{I}}_4A_4)\cdot\hat{\mathbf{S}}_{(Mn)_4} + \frac{1}{2}D\frac{3\cos^2\theta - 1}{3}(\hat{\mathbf{S}}_z^2 - \hat{\mathbf{S}}^2) - J(\hat{\mathbf{S}}^2 - 1)$$

where both interacting electronic spins are $^1/_2$. Both g tensors are isotropic with g values of 2.0046 and 1.995 for the tyrosine and the manganese cluster, respectively. We include the hyperfine term for the manganese cluster, which has an important contribution (see below). On the other hand, the hyperfine term for $Y_z^{\bullet}$ was neglected because the known coupling constants are considerably less than the 23 mT line width of the split feature. The isotropic hyperfine coupling constants for the four manganese ions were taken from simulations of the normal multiline signal (12.25, 9.37, 8.60, and 3.76 mT).[24] D is the dipolar coupling constant given by eq 1.[25] θ is the angle between the magnetic field direction and the axis

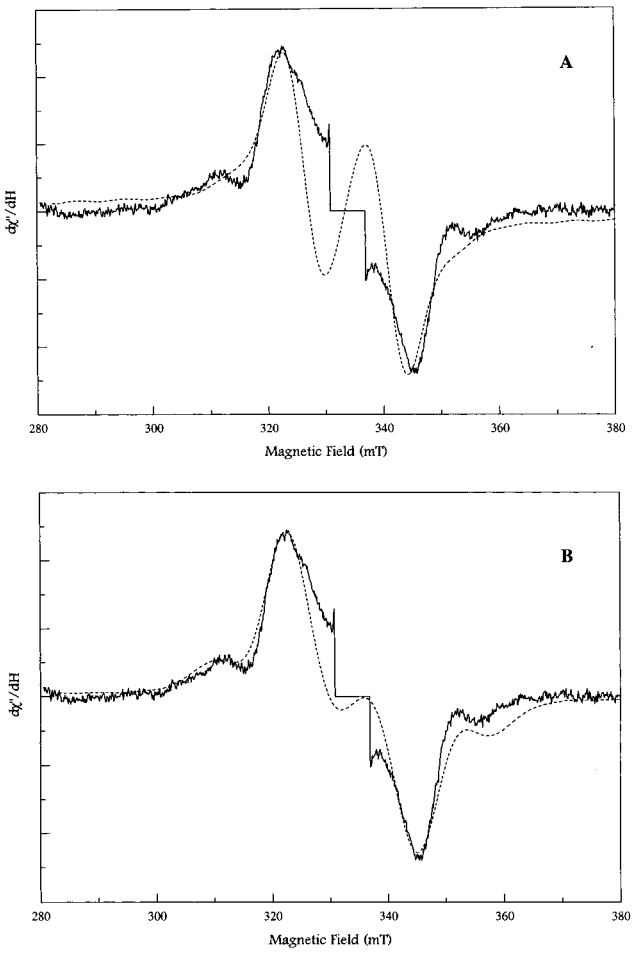

Figure 2. (−) Light minus-annealed CW-EPR spectrum of the $S_2Y_z^{\bullet}$ state in acetate-treated BBY membrane. Experimental conditions: $\nu_{mw} = 9.4699$ GHz; power = 7.93 mW; modulation amplitude = 5 G; time constant = 40 ms; scan time = 80 s; $T = 15$ K; one scan. (- - -) Simulated spectra: (A) dipolar interaction only, $D = -673$ MHz, $J = 0$ MHz; (B) exchange interaction only, $D = 0$ MHz, $J = -406$ MHz.

$$D = -\frac{3\mu^{\circ}}{8\pi}(g_e\beta_e)^2\frac{1}{r^3} \qquad (1)$$

joining the two dipoles (dipolar axis), and J is the exchange coupling constant representing, in the definition used here, one-half of the energy gap between the singlet and the triplet states as a result of the exchange interaction. The exchange coupling is taken as isotropic, and J is generally assumed to depend exponentially on the distance, eq 2.[26] Typical values for J_o and

$$J = J_o\exp\left(-\frac{r}{r_o}\right) \qquad (2)$$

r_o range from 10^{11} to 10^{12} G and 0.3 to 0.5 Å, respectively.

The Hamiltonian was evaluated with the method in ref 27. The eigenvectors and eigenvalues of the Hamiltonian are

$$|\Phi_1\rangle = |T_1\rangle \qquad \omega_1 = \omega - J + D_{zz}/2$$

$$|\Phi_2\rangle = \cos\Psi\,|S\rangle + \sin\Psi\,|T_0\rangle \qquad \omega_2 = \Omega - D_{zz}/2$$

$$|\Phi_3\rangle = -\sin\Psi\,|S\rangle + \cos\Psi\,|T_0\rangle \qquad \omega_3 = -\Omega - D_{zz}/2$$

$$|\Phi_4\rangle = |T_{-1}\rangle \qquad \omega_4 = -\omega - J + D_{zz}/2$$

with:

$$\omega = \frac{1}{2}(\omega_{Y_z} + \omega_{(Mn)_4}) \quad \Omega^2 = \left(J + \frac{1}{2}D_{zz}\right)^2 + Q^2$$

$$\omega_{Y_z} = \frac{g_{Y_z}\beta H}{\hbar} \qquad \omega_{(Mn)_4} = \frac{g_{(Mn)_4}\beta H}{\hbar} + (m_{I_1}A_1 + m_{I_2}A_2 + m_{I_3}A_3 + m_{I_4}A_4)$$

$$D_{zz} = \frac{2}{3}D \qquad Q = \frac{1}{2}(\omega_{Y_z} - \omega_{(Mn)_4})$$

$$\tan 2\psi = \frac{(\omega_{Y_z} - \omega_{(Mn)_4})}{2J + D_{zz}}$$

The frequencies of the four different EPR transitions and their corresponding transition probabilities are given by

$$\omega_{12_{Mn}} = \omega - \Omega - J + D_{zz} \quad P_{12} = (2\Omega + 2J + D_{zz})/(4\Omega) \tag{3-1}$$

$$\omega_{34_{Mn}} = \omega - \Omega + J - D_{zz} \quad P_{34} = (2\Omega - 2J - D_{zz})/(4\Omega) \tag{3-2}$$

$$\omega_{13_{Yz}} = \omega + \Omega - J + D_{zz} \quad P_{13} = (2\Omega - 2J - D_{zz})/(4\Omega) \tag{3-3}$$

$$\omega_{24_{Yz}} = \omega + \Omega + J - D_{zz} \quad P_{24} = (2\Omega + 2J + D_{zz})/(4\Omega) \tag{3-4}$$

The labels Mn or Yz indicate to which system, manganese cluster or tyrosyl radical, the transition belongs in the absence of interaction. For the coupled system, the EPR transitions, calculated by using eqs 3-1 to 3-4, were convoluted with normalized Gaussian line shapes with line widths chosen to account for the inhomogeneous broadening due to spin−spin relaxation and unresolved hyperfine coupling. The intensity of each transition is proportional to the difference in populations of the two states between which the transition takes place, scaled by the corresponding transition probability. The spectra for the randomly oriented spin systems were obtained by spherical averaging over the angle θ.

Simulations of the split signal were first carried out by using pure dipolar coupling, $J = 0$ (Figure 2A), or pure exchange coupling, $D = 0$ (Figure 2B), to describe the electron spin−spin interaction. The satellite peaks were predicted by our simulations only for cases in which the exchange interaction was nonzero. When the spin−spin coupling was modeled by a pure dipolar interaction ($J = 0$), the Pake pattern expected with parallel and perpendicular components was broadened by the hyperfine interaction of the manganese cluster. When the spin−spin coupling was modeled entirely by isotropic exchange, no satellite peaks were expected a priori. However, in this case, the influence of the hyperfine interaction of the manganese cluster is strong enough to split the tyrosine signal further. This can be seen from eqs 3-1 to 3-4 for the resonance frequencies of the interacting system. When J is small, Ω is almost equal to Q and $\omega_{13_{Yz}}$ and $\omega_{24_{Yz}}$ only contain the Zeeman term of the tyrosine. When J increases, the hyperfine term for the manganese cluster contributes to the resonance frequencies through Ω.

These model simulations show that the interaction between the manganese cluster and the tyrosyl radical is predominantly exchange. However, because of the distance dependence of the parameters J and D, a dipolar contribution must also be present (see Discussion). New simulations were, thus, carried out by increasing the parameter D value until distortions started to appear in the shape of the signal; this approach provided an upper limit for the magnitude of the dipolar coupling. These simulations are shown in Figure 3A for the signal obtained with PS II membranes. The values obtained for the coupling constants are, respectively, −392 MHz for J and −140 MHz for D. Using eq 1, we find a distance of 8.2 Å between the two spins. A comparison with values reported for exchange coupling in the literature[26b] shows that such a distance is also compatible with the value found for J.

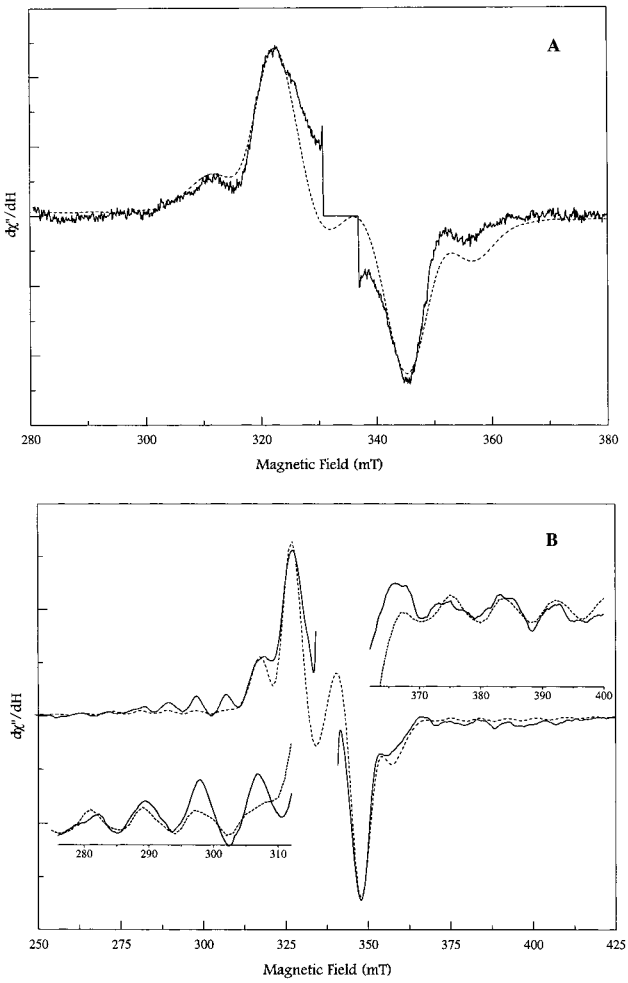

Figure 3. (A) Experimental (—) and simulated (- - -) CW-EPR spectrum of the $S_2Y_z^\bullet$ state in acetate-treated BBY membrane. Experimental conditions as in Figure 2. Simulations parameters: $D = -140$ MHz, $J = -392$ MHz. (B) Experimental (—) and simulated (- - -) CW-EPR spectrum of the $S_2Y_z^\bullet$ state in acetate-treated RCC. Experimental conditions as in Figure 1. Simulations parameters: $D = -112$ MHz, $J = -350$ MHz. The insets show expansions of the underlying multiline (the simulated spectrum has been scaled by a factor of 2 for comparison in the two insets).

As mentioned above, the spectrum of the $S_2Y_z^\bullet$ species exhibits an underlying multiline signal due to ^{55}Mn hyperfine couplings. To check the consistency of our simulations with respect to this signal, we modified the program file to allow the use of two different line widths in the convolution of the stick spectrum and new simulations were carried out. The result is shown in Figure 3B for the signal obtained in RCCs. It was indeed possible to reproduce the features of the experimental spectrum. Although the intensity of the underlying multiline is weak in the simulations (due in part to the use of simplified formulas for the transition probabilities in the model chosen here), the positions of the lines were reproduced correctly,

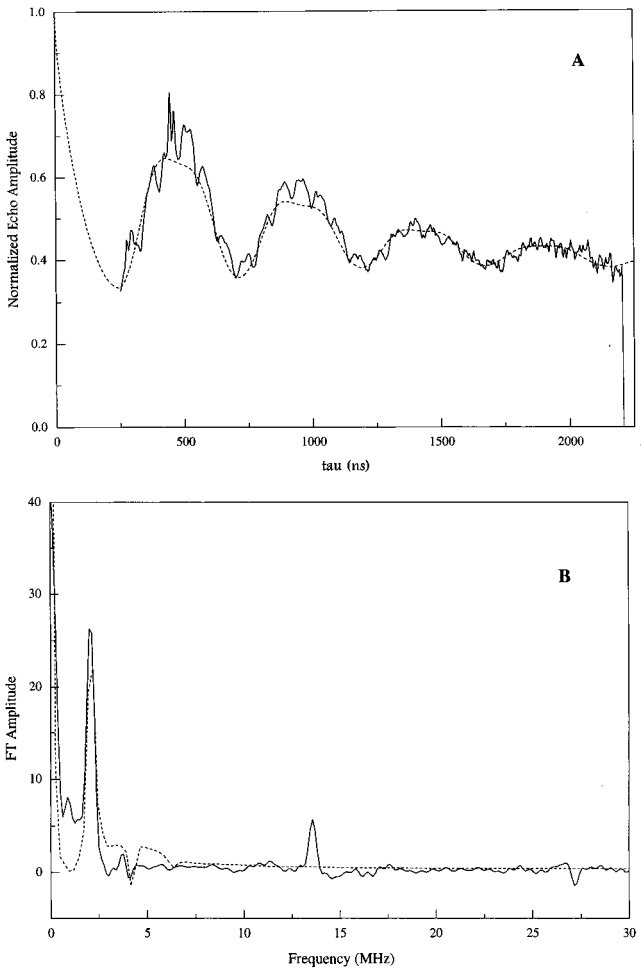

Figure 4. Experimental (—) and simulated (- - -) two-pulse ESEEM data recorded for the $S_2Y_z^\bullet$ signal in acetate-treated PSII RCCs. (A) Time-domain spectrum obtained from the dark minus-annealed data. Experimental conditions: $\nu_{mw} = 8.820$ GHz; $H_o = 320$ mT; MW power = 40−50 W; starting $\tau = 248$ ns; time increment = 4 ns; repetition rate = 60 Hz; $T = 1.8$ K. Simulation parameters ($S = {}^1/_2$, $I = 1$, ^{2}H nucleus): $A_{iso} = 0$ MHz; $T_{dip} = 0.42$ MHz; $e^2qQ = 0.25$ MHz; $\eta = 0$. The decay function was modeled by $V_{decay} = \exp(-\tau/\tau_o)^{0.5}$ with $\tau_o = 900$ ns. (B) Corresponding frequency domain of the two-pulse data obtained by Fourier transformation of the time domain.

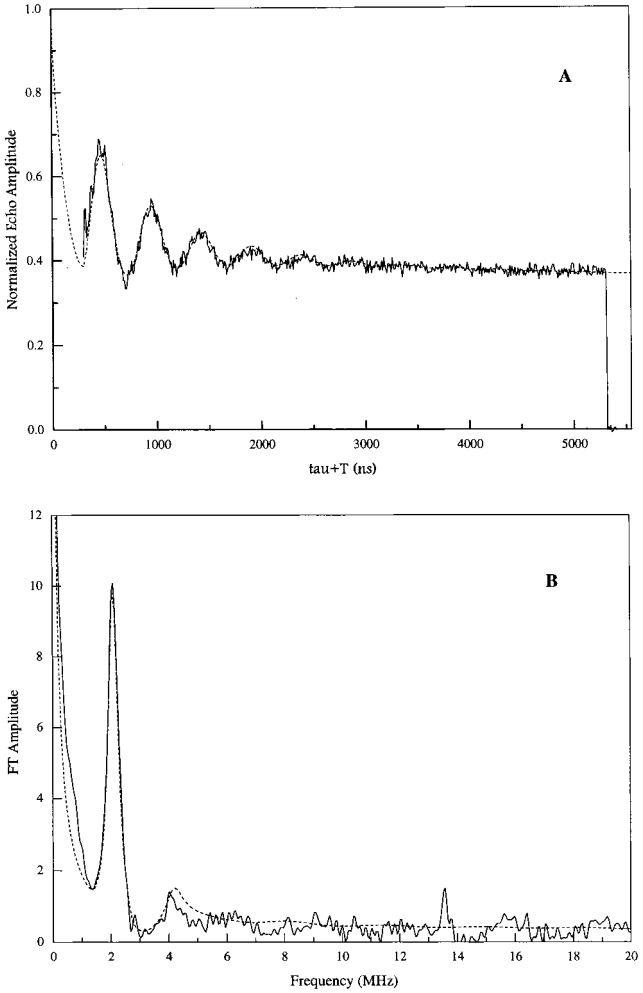

Figure 5. Experimental (—) and simulated (- - -) three-pulse ESEEM data recorded for the $S_2Y_z^\bullet$ signal in acetate-treated PSII RCCs. (A) Time-domain spectrum obtained from the dark minus-annealed data. Experimental conditions: $\nu_{mw} = 8.820$ GHz; $H_o = 320$ mT; MW power = 40−50 W; $\tau = 239$ ns; starting $T = 61$ ns; time increment = 10 ns; repetition rate = 60 Hz; $T = 1.8$ K. Simulation parameters ($S = {}^1/_2$, $I = 1$, ^{2}H nucleus): $A_{iso} = 0$ MHz; $T_{dip} = 0.42$ MHz; $e^2qQ = 0.25$ MHz; $\eta = 0$. The decay function was modeled by $V_{decay} = \exp(-(\tau + T)/\tau_o)^{0.5}$ with $\tau_o = 1.1$ μs. (B) Corresponding frequency domain of the three-pulse data obtained by Fourier transformation of the time domain.

showing that the interaction between S_2 and $Y_z^\bullet$ is responsible for the shift in apparent hyperfine coupling observed for $S_2Y_z^\bullet$ compared to the normal multiline. The values obtained for J and D (−350 and −112 MHz, respectively) are lower than those obtained by simulating the signal from acetate-treated BBYs, in agreement with the narrower splitting observed in cores. The D value leads to a dipole−dipole distance of 8.9 Å.

ESEEM. The ESEEM data for $S_2Y_z^\bullet$ were collected 5 mT upfield from the center of the $Y_D^\bullet$ absorption signal. The time-domain data set recorded for the annealed sample was subtracted from the time-domain data set recorded for the illuminated sample, and the resulting difference was then normalized. Figures 4A and 5A show these normalized time-domain ESEEM data obtained for two-pulse and three-pulse experiments on the $S_2Y_z^\bullet$ signal generated in deuterated samples. Both data sets are dominated by ESEEM arising from ^{2}H weakly coupled to the $S_2Y_z^\bullet$ paramagnetic center. Figures 4B and 5B show the cosine Fourier transform of the time-domain data. The resulting two-pulse frequency domain spectrum exhibits a positive peak at 2.09 MHz, the ^{2}H Larmor frequency at 320 mT, and a ^{2}H sum combination peak at 4.2 MHz, which is marked by the opposite phase.[28] Also observed are a positive peak at 13.6 MHz and a negative peak at 27.2 MHz that arise from weakly coupled protons. The three-pulse frequency domain spectrum (Figure 5B) presents prominent peaks at 2.09 and 13.6 MHz and a smaller one at 4.2 MHz. This last peak is also a ^{2}H-combination line but one that results from the presence of multiple deuterium nuclei coupled to the unpaired electron spin.[29] These data were first obtained and reproduced in reaction center cores. To check if there is any dependence with respect to the polypeptide and membrane composition of the sample, a three-pulse experiment was carried out on an acetate-treated BBY sample under the same experimental conditions. The time-domain spectrum obtained was essentially identical to that obtained with cores (see Figure 6).

A detailed analysis of the ^{2}H-ESEEM data of Figures 4 and 5 allows us to determine the number of exchangeable deuterons coupled to $S_2Y_z^\bullet$ and their distances from the paramagnetic center. For the dipolar- or matrix-coupled deuterons of interest here, the modulation depth, or amplitude, is a function of the number of coupled nuclei divided by their dipole−dipole distance raised to the sixth power.[28] The damping of each modulation frequency component is derived from magnetic

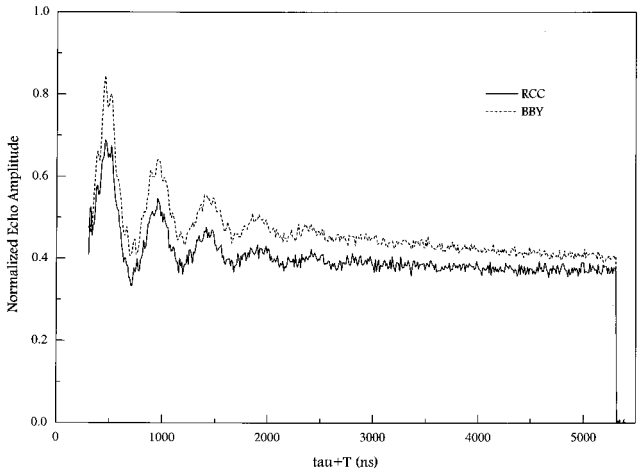

Figure 6. Experimental three-pulse ESEEM time-domain data recorded for the $S_2Y_z^{\bullet}$ signal in both acetate-treated PSII RCCs and BBYs. The spectrum for RCCs is the same as in Figure 5A; experimental conditions are the same for the data recorded on BBYs and RCCs. The difference displayed is mostly derived from background decay of the modulation function and not differences in hyperfine coupling.

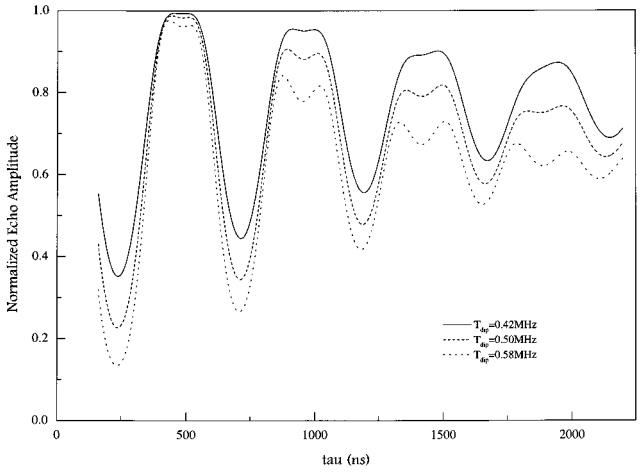

Figure 7. Simulated traces for a two-pulse ESEEM experiment ($S = {}^1/_2$, $I = 1$) showing the effect of the coupling on the second harmonic component. Parameters (^{2}H nucleus): $H_o = 320$ mT; starting $\tau = 248$ ns; $A_{iso} = 0$ MHz; $e^2qQ = 0.25$ MHz; $\eta = 0$; T_{dip} as indicated.

interactions that broaden the hyperfine interaction, e.g., the electron−nuclear dipole−dipole coupling, and the "background" decay of the electron spin−echo that arises from spin relaxation processes. For two-pulse data, the background decay is governed by the inhomogeneous electron spin−spin relaxation time and can be a major contributor to the damping. To remove this background decay, the overall two-pulse ESEEM data were fit with a normalized second-order polynomial function and then divided by this function to yield the ESEEM function shown in Figure 4A.

An additional piece of information that is found in the two-pulse ESEEM data of electron spin $^1/_2$ systems concerns the relative damping of the fundamental ^{2}H modulation frequency at 2.1 MHz with respect to that of the sum combination feature at 4.2 MHz. Because the dipolar contribution to the line width of the ESEEM peaks is of opposite sign in the two electron-spin manifolds that combine to yield the sum-combination peak, the damping, or line width, of this component is dominated by the deuterium nuclear quadrupole interaction.[30] Therefore, the relative damping of these two frequency components becomes important for analyses of problems such as the one studied here, because it provides an extra constraint for simulations that is independent of the procedure used to remove the background decay from the data. The two-pulse ^{2}H-ESEEM simulations shown in Figure 7 illustrate how varying the strength of the electron−nuclear dipole−dipole interaction affects the amplitude and damping of the modulations. For $T_{dip} = 0.58$ MHz (dashed line), the fundamental frequency component damps quickly, leaving the sum-combination frequency clearly visible at longer times. When T_{dip} is lowered to 0.42 MHz (solid line), the depth of the modulations decreases along with the damping of the fundamental deuterium frequency. As a result, the sum-combination frequency is less prominent in the data at longer values of τ. A comparison of these simulations with the two-pulse ^{2}H-ESEEM data of Figure 4A shows that the data are most consistent with the features of the ESEEM function predicted for the smaller dipole−dipole coupling. Using 0.42 MHz for T_{dip} and an $S = {}^1/_2$, $I = 1$ model for ESEEM simulations, four coupled deuterons are required to achieve the modulation depth found in the experiment. The results of these calculations are shown by the dashed curves in Figure 4 and for the stimulated echo data in Figure 5.

A close examination of Figure 4B reveals that even for the smaller dipole−dipole coupling, $T_{dip} = 0.42$ MHz, the intensity of the sum-combination peak predicted is greater than that observed. This is most likely a consequence of the $S = 1$ nature of the $S_2Y_z^{\bullet}$ species. Sloop et al. have shown that for an $S = 1$ electron-spin system coupled to an $I = {}^1/_2$ nucleus, the two-pulse modulation function takes the form:

$$E_{mod}(\tau) = 1 - 2K[\sin^2(\omega_{1/-1}\tau/2)\sin^2(\omega_I\tau/2)] \quad (4)$$

$$K = \{[2B(\omega_{1/-1} + \omega_I + A)]/[B^2 + (\omega_{1/-1} + \omega_I + A)^2]\}^2 \quad (5)$$

where K is the modulation depth parameter, ω_1 and ω_{-1} are the hyperfine frequencies for the coupled nucleus in $|T_1\rangle$ or $|T_{-1}\rangle$ electron-spin manifolds, and ω_I is the nuclear Larmor frequency that represents the chief nuclear interaction for the $|T_0\rangle$ level where the hyperfine coupling vanishes.[31] For each EPR transition, two-pulse ESEEM data will show four frequency components: a hyperfine frequency, ω_+ or ω_- from either the $|T_+\rangle$ or $|T_-\rangle$ electron-spin manifolds; a peak at the nuclear Larmor frequency, ω_I, from the central electron-spin level, where $m_S = 0$; and combination frequencies at $\omega_\pm + \omega_I$ and $\omega_\pm - \omega_I$. Because the hyperfine anisotropy is only contained in ω_+ or ω_-, the sum-combination peak will be characterized by the same damping as the fundamental.[32] This is the most likely cause of the reduced contribution of the deuterium sum-combination feature in Figure 4A. Because the modulation depth parameter, K, also differs from that determined for $S = {}^1/_2$, $I = {}^1/_2$ systems, caution must be exercised when considering the above computer simulations and those published previously.

Discussion

CW EPR Simulations. Several simulations of the $S_2Y_z^{\bullet}$ signal that model the electron spin−spin coupling with dominant dipolar- or isotropic-exchange interactions already exist in the literature.[2a,8−10] Our results show that a pure dipolar interaction is not possible because it does not account for the satellite peaks observed in acetate-treated preparations. A large isotropic exchange coupling is required in order to simulate these features. Simulations that consider only an electron−electron dipolar interaction require a large coupling (D of at least −670 MHz),

which implies a short distance between the two interacting species and, thus, overlap of their orbitals. Such orbital overlap, however, will produce a significant exchange interaction. On the other hand, using a pure exchange coupling is not relevant either. Studies of exchange couplings in several systems have led to an exponential dependence of the interaction strength with the distance;[26] the *J* coupling essentially disappears for distances greater than about 12 Å. At this distance the dipolar interaction, which varies in proportion to the inverse of the cubic distance, is still nonzero. A dipolar contribution must, therefore, be included in the simulations. It has been suggested[2a,9] that the dipolar term would be averaged out by relaxation mechanisms when higher spin states of the $(Mn)_4$ cluster are thermally populated. The energy difference between the ground state and the first excited state of the cluster has been estimated to be 36.5 cm^{-1} [33] in the functional system, and this value is close in acetate-treated samples (about 42 cm^{-1}),[34] hence only the ground state will be populated significantly at the temperature at which spectra of the $S_2Y_z^{\bullet}$ species are routinely recorded. Also, the fast relaxation of the cluster, induced when one increases the temperature, averages out not only the dipolar interaction but also the exchange coupling between the two species.[35]

A second important feature revealed by our simulations is the dramatic change in the transition probabilities caused by the exchange and dipolar interactions. As seen from eqs 3-1 to 3-4, these probabilities depend directly on the parameters *D* and *J* and results in a redistribution of the microwave absorption spectrum. This, in turn, influences spin quantifications of the split signal, when the narrow $Y_D^{\bullet}$ signal is used as a spin standard.[12,36] In the area around $g = 2$, the interaction mixes the wave functions of the tyrosine and manganese cluster spin centers. Under these conditions, it is not possible to say which signal belongs to the radical and which signal comes from the cluster. Our simulations show that the cluster has a fair contribution to the $S_2Y_z^{\bullet}$ signal in the $g = 2.0$ region in the case of the acetate-treated sample. We estimate from these simulations that the area of the $Y_D^{\bullet}$ signal, which represents one spin per reaction center, is only about 60% of the area of the main split signal (the two main peaks plus the two satellite peaks, the underlying multiline being subtracted out). Hence, spin quantification of the $S_2Y_z^{\bullet}$ signal with $Y_D^{\bullet}$ as a standard presents an upper limit of the amount trapped. However, in systems with a narrower splitting than in acetate-treated samples, as in calcium- or chloride-depleted PS II, the interaction is less strong and the error made becomes smaller.

The distance of 8.2−8.9 Å found with the simulations is the magnetic distance between the center of the spin density of the tyrosine radical and the center of the spin density of the manganese cluster. In the approach we have used, the dipolar term has axial symmetry and we have assumed the point-dipole approximation. Given the distance found and the size of the manganese cluster, we note that this approximation may not be fully relevant in this case and, thus, we have a lower limit for the distance separating the two species. However, it is sufficient for the purpose of these simulations to show that the interaction is primarily exchange in acetate-treated samples. A second assumption we have made is the orientation independence of the exchange coupling. This is a very good model in liquids because fast motion averages anisotropic interactions to zero, but in the case of large proteins, such as photosystem II, this may not be the case. There is no fundamental reason for the exchange interaction to be isotropic. Unfortunately, however, very little is known about its anisotropy and we are not aware of any good model to account for it.

There is also an uncertainty about the hyperfine values for the $(Mn)_4$ cluster. They are not known accurately, and we have not attempted to vary them here to get a better fit. Our aim is to show that the hyperfine term in the Hamiltonian has a significant role in producing the shoulders that are observed on the split signal in acetate-treated samples and also that it is possible, with the model chosen for the simulations, to reproduce the change induced by the $S_2Y_z^{\bullet}$ interaction in the line positions of the underlying multiline signal compared to the normal multiline. Although no multiline is observed in acetate-treated samples upon illumination at low temperature, we have used hyperfine values obtained by simulations of the normal multiline. The basis of this choice lies in observations by Brudvig and co-workers[22,34] who found that, in the presence of NO, the generation of the $S_2Y_z^{\bullet}$ species in acetate-treated samples leads to an S_2Y_z−NO adduct that exhibits a multiline signal very similar to the normal multiline. Concerning the strength of the interaction and the relative contributions of exchange and dipolar couplings, we found that the exchange parameter *J* has the largest influence on the observed splitting in the $S_2Y_z^{\bullet}$ signal. This result was already obtained by MacLachlan et al. in their simulations of various split signals.[10] Here, we have carried the analysis further by looking at the relative distance dependence of the parameters *J* and *D* to keep them in agreement and also by trying to simulate the underlying multiline signal present in acetate-treated samples. This attempt to simulate the full signal in the acetate-treated sample allows us to stress the importance of the coupling and that the radical and the cluster must be treated together and regarded as one entity in this state. Fitting signals of the $S_2Y_z^{\bullet}$ state with decreasing splitting (acetate-treated BBYs, acetate-treated RCCs, calcium-depleted preparations) while keeping *J* and *D* consistent with their distance dependence required changes primarily in the exchange-coupling value while the parameter *D* remained essentially constant. For example, we were able to simulate the split signal exhibited in Ca^{2+}-depleted salt-washed BBYs with the following parameters: $J = -123$ MHz and $D = -106$ MHz (data not shown) for a splitting of 14.5 mT. As the splitting decreases, the exchange character of the interaction becomes less marked. In terms of distances, however, these changes in line shape as a function of preparation or inhibitory treatment translate to a variation of less than 1 Å for the dipole−dipole distance.

ESEEM. The deuterium modulation observed in our experiments can arise from ^2H_2O molecules that are bound to $S_2Y_Z^{\bullet}$, from exchangeable deuterons of the radical pair and the region of the protein close enough to couple to the $S_2Y_Z^{\bullet}$ species, and from ambient water molecules that are close to the paramagnetic center. Because the deuterium modulation depth is a function of both the number of coupled nuclei and their dipole−dipole distance, the damping of the modulation, which is governed primarily by the electron−nuclear dipole−dipole distance, needs to be incorporated into the analysis to differentiate between various models. For both two- and three-pulse data, background decay functions that depend on electron spin relaxation processes must be deconvoluted from the damping to permit this analysis. For $S = {}^1/_2$ systems, the best way to achieve this goal is by analyzing two-pulse data where the relative damping between the ^2H-fundamental and sum-combination peaks can be used as an independent observable for determining the dipole−dipole distance. Our analysis above, however, indicates that the two-pulse ESEEM damping may not be adequately modeled as a ficticious $S = {}^1/_2$ system. The two-pulse ESEEM data from a radical pair like $S_2Y_Z^{\bullet}$ is expected to bear some resemblance to the organic triplet species studied by Sloop et al.[31,32] Because

the observed EPR transitions for $S_2Y_Z^\bullet$ will involve one of the electron-spin sublevels where $m_S = 0$, the deuterium fundamental modulation component and the sum combination feature will both be broadened to the same extent by the electron−nuclear dipolar interaction. As a result, resolution of the ambiguity between the number of coupled deuterons and their dipolar distances from $S_2Y_Z^\bullet$ will have to rest on a more tenuous modeling of the ^{2}H-ESEEM damping.

The work of Sloop et al. showed that it is not just the damping characteristics that differ for the ESEEM of an $S = 1$ system but that the modulation depth is also affected.[31] The triplet can only be treated as a fictitious $S = {}^1/_2$ system when one of the EPR transitions can be selectively probed. Given that the isotropic exchange interaction found for $S_2Y_Z^\bullet$ in this work, −350 MHz for RCCs, is approximately an order of magnitude larger than the probing microwave field, the depth parameter derived for organic triplet states (eq 5) should provide a reasonable estimate for $S_2Y_Z^\bullet$ ESEEM near $g = 2.00$. This expression bears resemblance to that derived for an $S = {}^1/_2$, $I = {}^1/_2$ spin system and will collapse to an identical form for the weak coupling case where the nuclear Zeeman interaction dominates the nuclear spin Hamiltonian.

Our analysis strategy was to select the simplest model that accounted for the modulation depth and damping for both two- and three-pulse ESEEM data. Because the effects of the ESE background decay are most pronounced for the two-pulse data, it is most straightforward to remove it by performing a polynomial or exponential fit to the data and then dividing the resulting function into the experimental data. The results of such a procedure were shown for the two-pulse data displayed in Figure 4A. Removing the background decay from three-pulse data is more difficult. The approach taken in this work and in many of the quantitative ESEEM studies published in the literature has been to simulate the ESEEM function and then to use trial and error methods to approximate the background decay to facilitate a comparison between theory and experiment. The analysis in this paper is distinguished from those presented previously in that our simulations focused on two-pulse ESEEM data where the effects of background decay and hyperfine anisotropy are easier to resolve.

For the current study, the simplest $S = {}^1/_2$, $I = 1$ based model that accounted for the modulation depth and damping found for two- and three-pulse ESEEM data called for the inclusion of four coupled deuterons with an average T_{dip} of 0.42 MHz. The hyperfine coupling obtained for the four nuclei is an average value because the data do not carry enough spectral information to get an accurate distribution. Owing to this difficulty and the concerns above on the most rigorous way in which to treat the exchange-coupled systems, we defer to subsequent work a more detailed interpretation of the structural implications of this result. In similar spin−echo work on acetate-treated BBYs, Britt and co-workers simulated their data with two exchangeable deuterons with $T_{dip} = 0.57$ MHz.[8] In their analysis of three-pulse ESEEM data, these authors used the width of the deuterium ENDOR spectrum found for their ^{2}H-exchanged samples to fix an average dipole−dipole distance for ESEEM simulations and then varied the number of coupled deuterons at that distance to account for the ^{2}H-ESEEM depth.[8] Within the framework of an $S = {}^1/_2$, $I = 1$ model, a dipole−dipole interaction of 0.57 MHz predicts quicker damping of the fundamental frequency component than we observed in our experimental two-pulse ^{2}H ESE experiment.

In Ca^{2+}-depleted BBYs, two nuclei were needed to fit ESEEM data recorded for the $S_2Y_Z^\bullet$ species;[12] the T_{dip} value (0.48 MHz) was intermediate to the values reported here and by Force et al.[8] A significant difference between the acetate-treated and Ca^{2+}-depleted samples is that the dark-adapted, Ca^{2+}-depleted samples exhibit a dark-stable multiline signal from the $(Mn)_4$ cluster along with background signals whereas background signals only constitute the EPR spectrum of the annealed acetate-treated samples used here. In both types of samples, the data were corrected for dark signals and thus, in Ca^{2+}-depleted but not in the acetate-treated samples contributions from nuclei in the vicinity of the uncoupled $(Mn)_4$ cluster were subtracted from the coupled $S_2Y_Z^\bullet$ ESEEM data.

Conclusions

Simulations of the EPR spectra of the $S_2Y_Z^\bullet$ species detected in acetate-treated PSII preparations indicate that both dipolar and exchange interactions are involved in determining the line width of the observed signal. Mn hyperfine couplings contribute to the observed spectral line shape in an important way. Within the electron−electron point-dipole approximation used in our analysis, the distance between the tyrosyl radical and the $(Mn)_4$ cluster is 8−9 Å, consistent with recent models for the structure of the oxygen-evolving complex.[3] The EPR spectral simulations also show evidence for significant spin-coupled character in the $S_2Y_Z^\bullet$ system. This is an important observation and has not been recognized in earlier treatments of $S_2Y_Z^\bullet$. The ESEEM data that we have reported support the idea that spin coupling has significant effects on the Hamiltonian of ^{2}H nuclei coupled to the $S_2Y_Z^\bullet$ electron spins in acetate-treated samples. An analysis of the ESE data that is constrained by data from both two- and three-pulse ESEEM is consistent with the occurrence of four exchangeable deuterons in the close proximity of the cluster. The necessity of refining the EPR analysis by distributing the electron-spin density for the tyrosyl radical and the metal ions in the $(Mn)_4$ cluster and the ESE analysis by dealing with the spin-coupled character of the $S_2Y_Z^\bullet$ state is apparent and currently underway.

Acknowledgment. We acknowledge valuable discussions with Cecilia Tommos, and we thank Catherine DeMaso for help with the SDS-PAGE analysis. We thank Sun Un for useful discussions on coupled systems and simulations. This work was supported by the Human Research Frontiers program, by the USDA NRICRGP, and U.S. National Institutes of Health Grant Nos. GM-37300 (G.T.B.) and GM-54065 (J.M.). On the occasion of this special issue, J.M. and G.T.B. thank Ken Sauer and Mel Klein for their skills and qualities as teachers.

References and Notes

(1) (a) Britt, R. D. In *Oxygenic Photosynthesis: The Light Reactions*; Ort, D. R., Yocum, C. F., Eds.; Kluwer Academic Publishers: Dordrecht, 1996; pp 137−164. (b) Diner, B. A.; Babcock, G. T. In *Oxygenic Photosynthesis: The Light Reactions*; Ort, D. R., Yocum, C. F., Eds.; Kluwer Academic Publishers: Dordrecht, 1996; pp 213−247.

(2) (a) Gilchrist, M. L.; Ball, J. A.; Randall, D. W.; Britt, R. D. *Proc. Natl. Acad. Sci. U.S.A.* **1995**, *92*, 9545. (b) Tommos, C.; Tang, X. S.; Warncke, K.; Hoganson, C. W.; Styring, S.; McCracken, J.; Diner, B. A.; Babcock, G. T. *J. Am. Chem. Soc.* **1995**, *117*, 10325.

(3) (a) Hoganson, C. W.; Lydakis-Simantiris, N.; Tang, X. S.; Tommos, C.; Warncke, K.; Babcock, G. T.; Diner, B. A.; McCracken, J.; Styring, S. *Photosynth. Res.* **1995**, *46*, 177. (b) Babcock, G. T. In *Photosynthesis: From Light to Biosphere*; Mathis, P., Ed.; Kluwer Academic Publishers: Netherlands, 1995; Vol. II, p 209. (c) Babcock, G. T.; Espe, M.; Hoganson, C. W.; Lydakis-Simantiris, N.; McCracken, J.; Shi, W.; Styring, S.; Tommos, C.; Warncke, K. *Acta Chem. Scand.* **1997**, *51*, 533. (d) Hoganson, C. W.; Babcock, G. T. *Science* **1997**, *277*, 1953. (e) Tommos, C.; Babcock, G. T. *Acc. Chem. Res.* **1998**, *31*, 18.

(4) Dismukes, G. C.; Siderer, Y. *Proc. Natl. Acad. Sci. U.S.A.* **1981**, *78*, 274.

(5) Boussac, A.; Rutherford, A. W. *Biochemistry* **1989**, *27*, 3476.
(6) Boussac, A.; Zimmermann, J.-L.; Rutherford, A. W. *Biochemistry* **1989**, *28*, 8984.
(7) Tang, X. S.; Randall, D. W.; Force, D. A.; Diner, B. A.; Britt, R. D. *J. Am. Chem. Soc*. **1996**, *118*, 7638.
(8) Force, D. A.; Randall, D. W.; Britt, R. D. *Biochemistry* **1997**, *36*, 12062.
(9) Boussac, A.; Zimmermann, J.-L.; Rutherford, A. W.; Lavergne, J. *Nature* **1990**, *347*, 303.
(10) MacLachlan, D. J.; Nugent, J. H. A.; Warden, J. T.; Evans, M. C. W. *Biochim. Biophys. Acta* **1994**, *1188*, 325.
(11) (a) Sinclair, J. *Biochim. Biophys. Acta* **1984**, *764*, 247. (b) Sandusky, P. O.; Yocum, C. F. *Biochim. Biophys. Acta* **1986**, *849*, 85.
(12) Tommos, C.; McCracken, J.; Styring, S.; Babcock, G. T. *J. Am. Chem. Soc.*, in press.
(13) (a) Berthold, D. A.; Babcock, G. T.; Yocum, C. F. *FEBS Lett.* **1981**, *277*, 69. (b) Ghanotakis, D. F.; Topper, J.; Babcock, G. T.; Yocum, C. F. *Biochim. Biophys. Acta* **1984**, *767*, 524.
(14) Mishra, R. K.; Ghanotakis, D. F. *Photosynth. Res.* **1994**, *42*, 37.
(15) McCracken, J. L.; Shin, D.-H.; Dye, J. L. *Appl. Magn. Reson.* **1992**, *3*, 305.
(16) Lin, C. P.; Bowman, M. K.; Norris, J. R. *J. Magn. Reson.* **1985**, *65*, 369.
(17) Britt, R. D.; Klein, M. P. *J. Magn. Reson.* **1987**, *74*, 535.
(18) Mims, W. B.; Peisach, J. In *Biological Magnetic Resonance;* Berliner, L. J., Ruben, J., Eds.; Plenum Press: New York, 1981; pp 213−263.
(19) Mims, W. B.; Peisach, J. In *Advanced EPR: Applications in Biology and Biochemistry* Hoff, A. J., Ed.; Elsevier: Amsterdam, 1989; Chapter 1.
(20) Mims, W. B. *J. Magn. Reson.* **1984**, *59*, 291.
(21) (a) Mims, W. B. *Phys. Rev. B.* **1972**, *5*, 2409. (b) Mims, W. B. *Phys. Rev. B.* **1972**, *6*, 3543.
(22) Szalai, V. A.; Brudvig, G. W. *Biochemistry* **1996**, *35*, 15080.
(23) MacLachlan, J. D.; Nugent, H. A. *Biochemistry* **1993**, *32*, 9772.
(24) Kusunoki, M. *Chem. Phys. Lett.* **1992**, *197*, 108.
(25) (a) Weil, J. A.; Bolton, J. R.; Wertz, J. E. *Electron Paramagnetic Resonance*; Wiley-Interscience: New York, 1994; pp 155−157. (b) Atherton, N. M. *Principles of Electron Spin Resonance*; Ellis-Harwood PTR Prentice Hall: New York, 1993; pp 50−55.
(26) (a) De Kanter, F. J. J.; den Hollander, J. A.; Huizer, A. H.; Kaptein, R. *Mol. Phys.* **1977**, *34*, 857. (b) Coffman, R. E.; Buettner, G. R. *J. Phys. Chem.* **1979**, *83* (18), 2387.
(27) Hore, P. J. In *Advanced EPR: Applications in Biology and Biochemistry*; Hoff, A. J., Ed.; Elsevier: Amsterdam, 1989; Chapter 12.
(28) Mims, W. B.; Peisach, J.; Davis, J. L. *J. Chem. Phys.* **1977**, *66*, 5536.
(29) Kosman, D. J.; Peisach, J.; Mims, W. B. *Biochemistry* **1980**, *19*, 1304.
(30) Shubin, A. A.; Dikanov, S. A. *J. Magn. Reson.* **1983**, *52*, 1.
(31) Sloop, D. J.; Yu, H.-L.; Lin, T.-S.; Weissman, S. I. *J. Chem. Phys.* **1981**, *75*, 3746.
(32) Yu, H.-L.; Sloop, D. J.; Weissman, S. I.; Lin, T.-S.; Norris, J. R.; Bowman, M. K. *J. Phys. Chem.* **1982**, *86*, 4287.
(33) Lorigan, G. A.; Britt, R. D. *Biochemistry* **1994**, *33*, 12072.
(34) Szalai, V. A.; Kühne, H.; Lakshmi, K. V.; Brudvig, G. W. *J. Am. Chem. Soc*., submitted for publication.
(35) (a) Eaton, S. S.; Eaton, G. R. *Coord. Chem. Rev.* **1988**, *83*, 29. (b) Fielding, L.; More, K. M.; Eaton, G. R.; Eaton, S. S. *J. Am. Chem. Soc.* **1986**, *108*, 8194.
(36) Szalai, V. A.; Brudvig, G. W. *Biochemistry* **1996**, *35*, 1946.